STRUCTURAL BIOLOGY COMMUNICATIONS

ISSN 2053-230X

A promiscuous kinase inhibitor delineates the conspicuous structural features of protein kinase CK2a1

Masato Tsuyuguchi,[a] Tetsuko Nakaniwa,[b] Masaaki Sawa,[c] Isao Nakanishi[d] and Takayoshi Kinoshita[a]*

[a]Graduate School of Science, Osaka Prefecture University, 1-1 Gakuen-cho, Naka-ku, Sakai, Osaka 599-8531, Japan, [b]Institute for Protein Research, Osaka University, Suita, Osaka 565-0871, Japan, [c]Carna BioSciences, Kobe, Hyogo 650-0047, Japan, and [d]Department of Pharmaceutical Sciences, Kindai University, 3-4-1 Kowakae, Higashi-osaka, Osaka 577-8502, Japan. *Correspondence e-mail: kinotk@b.s.osakafu-u.ac.jp

Received 22 May 2019
Accepted 22 June 2019

Edited by A. Nakagawa, Osaka University, Japan

Keywords: protein kinase CK2; ATP-analogue inhibitor; selectivity; off-target kinases; structural comparison.

PDB reference: CK2a1, complex with 5-iodotubercidin, 6jwa

Supporting information: this article has supporting information at journals.iucr.org/f

Protein kinase CK2a1 is a serine/threonine kinase that plays a crucial role in the growth, proliferation and survival of cells and is a well known target for tumour and glomerulonephritis therapies. Here, the crystal structure of the kinase domain of CK2a1 complexed with 5-iodotubercidin (5IOD), an ATP-mimetic inhibitor, was determined at 1.78 Å resolution. The structure shows distinct structural features and, in combination with a comparison of the crystal structures of five off-target kinases complexed with 5IOD, provides valuable information for the development of highly selective inhibitors.

1. Introduction

Protein kinase CK2a1 is a serine/threonine protein kinase that regulates the growth, proliferation and survival of a variety of cells. CK2a1 is an important target protein in serious diseases such as cancer and glomerulonephritis (Duncan & Litchfield, 2008; Yamada *et al.*, 2005). Structural studies of CK2a1 have contributed to the production of potent inhibitors, including CX-4945, the first clinical CK2a1 inhibitor (Siddiqui-Jain *et al.*, 2010).

In the development of antikinase drugs, researchers are faced with selectivity issues against off-target kinases. Crystal structures of target kinases serve to increase the potency of inhibitors, but are insufficient for obtaining high selectivity. Occasionally, comparative structural dissections lead to a drastic enhancement in the inhibitory selectivity between the target kinase and off-target kinases. Furthermore, common and/or disparate insights into the binding mode of a particular compound to protein kinases may confer clues for the development of highly selective inhibitors. Crystal structures of Src-family kinases with staurosporine, a well known broad-spectrum kinase inhibitor, provided structural insights that have enhanced the understanding of inhibitory selectivity in the Src family (Kinoshita *et al.*, 2006; Miyano *et al.*, 2009).

Here, we report the crystal structure of CK2a1 in complex with 5-iodotubercidin (5IOD) [Fig. 1(*c*)], an ATP-mimetic inhibitor, at 1.78 Å resolution. Comparative structural analyses of the complexes of 5IOD with CK2a1, CK1g2 (unpublished, but available in the Protein Data Bank), ERK1 (Kinoshita *et al.*, 2008), ERK2 (Kinoshita *et al.*, 2016), haspin (Eswaran *et al.*, 2009) and CLK1 (Heroven *et al.*, 2018)

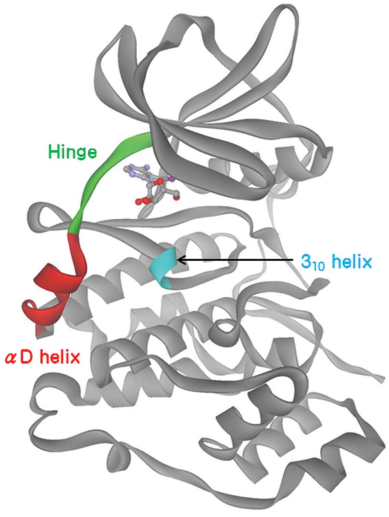

provided valuable structural insights for structure-based drug discovery of novel CK2a1-selective inhibitors.

2. Materials and methods

2.1. Macromolecule production

Recombinant human CK2a1 was prepared according to a previously reported protocol (Kinoshita *et al.*, 2013). The gene coding for human CK2a1 (1–335) was cloned into the pGEX-6P-1 vector (GE Healthcare) at BamHI and EcoRI restriction sites. *Escherichia coli* strain HMS174 (DE3) cells (Novagen) were transformed with the cloned plasmid and cultured in LB medium supplemented with 100 µg ml^{-1} ampicillin. Protein expression was induced with 0.2 m*M* isopropyl *β*-D-1-thio-galactopyranoside and the cells were incubated at 298 K for a further 15 h. The cells were harvested, resuspended in a buffer consisting of 150 m*M* NaCl, 25 m*M* Tris–HCl pH 7.4 and sonicated. After removing the cellular debris by centrifugation, the supernatant was loaded onto glutathione Sepharose 4B resin (GE Healthcare) and the CK2a1 protein was digested with 80 U ml^{-1} PreScission protease (GE Healthcare). The eluted CK2a1 was further purified by anion-exchange chromatography on a Mono Q column (GE Healthcare) using a linear gradient of 0–0.5 *M* NaCl in a buffer consisting of 25 m*M* Tris–HCl pH 8.0, 5 m*M* dithiothreitol.

2.2. Crystallization

The purified CK2a1 protein was concentrated to 5 mg ml^{-1} in anion-exchange elution buffer and used for crystallization. Prism-shaped crystals of apo CK2a1 were obtained by the sitting-drop vapour-diffusion method. Crystallization drops were prepared by mixing 2 µl protein solution with an equal volume of reservoir solution composed of 20–25% ethylene glycol as a precipitant and were equilibrated against 500 µl reservoir solution at 277 K. This condition was the same as the previous result (Sekiguchi *et al.*, 2009).

2.3. Data collection and processing

A piece of powdered 5-iodotubercidin (5IOD) with dimensions of approximately 0.1 mm (MedChemExpress) was placed into the crystallization drop. A large fraction of 5IOD remained in the solid state, and the subtly dissolved compound probably soaked into the apo CK2a1 crystals on storage overnight. The ethylene glycol used as a precipitant acted as a cryoprotectant. Diffraction data were collected using synchrotron radiation on beamline BL44XU at SPring-8 using an MX-300HE (Rayonix) detector. The X-ray diffraction set was processed and scaled using *HKL*-2000 (Otwinowski & Minor, 1997). Data-collection parameters and statistics are shown in Table 1.

2.4. Structure solution and refinement

Initial phasing was performed by the molecular-replacement method with *MOLREP* (Vagin & Teplyakov, 2010) using a previously reported structure of CK2a1 (PDB entry 3war; Kinoshita *et al.*, 2013) as the search model. Refinement, electron-density map calculations and model building were performed using *REFMAC*5 (Murshudov *et al.*, 2011), the *PHENIX* package (Adams *et al.*, 2010) and *Coot* (Emsley *et al.*, 2010). The refinement statistics are shown in Table 2. The

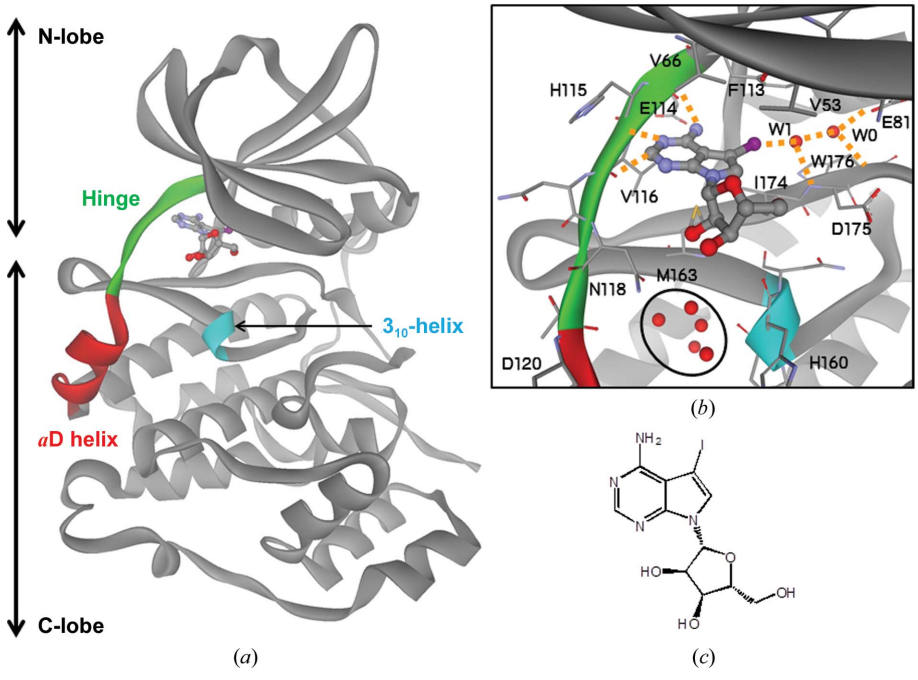

Figure 1
Crystal structure of 5-iodotubercidin (5IOD) bound to the ATP-binding site of CK2a1. (*a*) Overall structure of the 5IOD–CK2a1 complex. (*b*) Mode of interaction of 5IOD with CK2a1. Hydrogen bonds are shown as orange dotted lines. The clustered water molecules in the αD pocket are shown as red spheres and are circled. (*c*) Chemical structure of 5IOD.

Table 1
Data collection and processing.

Values in parentheses are for the outer shell.

Diffraction source	BL44XU, SPring-8
Wavelength (Å)	0.9
Temperature (K)	95
Detector	MX-300HE
Crystal-to-detector distance (mm)	250
Rotation range per image (°)	0.5
Total rotation range (°)	0–180
Exposure time per image (s)	0.5
Space group	$P2_12_12_1$
a, b, c (Å)	48.21, 78.94, 82.84
Mosaicity (°)	0.8
Resolution range (Å)	50.0–1.78 (1.81–1.78)
Total No. of reflections	224679
No. of unique reflections	30925
Completeness (%)	100 (100)
Multiplicity	7.3 (7.2)
$\langle I/\sigma(I)\rangle$	23.3 (2.5)
$R_{\rm r.i.m.}$†	0.103 (0.966)

† The redundancy-independent merging R factor $R_{\rm r.i.m.}$ was estimated by multiplying the conventional $R_{\rm merge}$ value by the factor $[N/(N-1)]^{1/2}$, where N is the data multiplicity.

Table 2
Structure solution and refinement.

Values in parentheses are for the outer shell.

Resolution range (Å)	50.00–1.78 (1.83–1.78)
Completeness (%)	100.0 (96.7)
No. of reflections, working set	28870 (2782)
No. of reflections, test set	1997 (189)
Final $R_{\rm cryst}$ (%)	18.5 (26.0)
Final $R_{\rm free}$ (%)	22.5 (32.1)
No. of non-H atoms	
Protein	2762
Ligand	44
Water	157
Total	2963
R.m.s. deviations	
Bonds (Å)	0.007
Angles (°)	1.047
Average B factors (Å^2)	
Protein	25.5
Ligand	26.0
Water	33.1
Ramachandran plot	
Most favoured (%)	96.92
Allowed (%)	2.46

final set of coordinates was deposited in the Protein Data Bank as entry 6jwa.

3. Results and discussion

3.1. Binding mode of 5-iodotubercidin to CK2a1

The crystal structure of CK2a1 adopts the conserved protein kinase fold, with the N-terminal and C-terminal lobes connected by the hinge region [Fig. 1(*a*)]. 5-Iodotubercidin (5IOD) binds to CK2a1 at the ATP-binding site, which is a hydrophobic groove located between the lobes [Fig. 1(*a*)]. The 4-aminopyrrolopyrimidine moiety of 5IOD is anchored by three hydrogen bonds to the carbonyl O atoms of Glu114 and Val116 and the NH group of Val116 in the hinge region, and the I atom forms a hydrogen bond to a water molecule (W1) ligated by the carbonyl O atom of Asp175 [Fig. 1(*b*)]. W1 also forms a hydrogen bond to a water molecule (W0) that is highly conserved among CK2a1 crystal structures and is ligated by the carbonyl O atom of Trp176 and the carboxyl group of Glu81. The pyrrolopyrimidine plane is bracketed by Val53, Val66, Met163 and Ile174 via hydrophobic interactions [Fig. 1(*b*)], resulting in the formation of a hydrophobic spine (C-spine) that is conserved among all kinases (Taylor & Kornev, 2011). The ribose moiety of 5IOD forms no hydrogen bonds to CK2a1, even though the ability of this moiety to form hydrogen bonds is high. Five clustered water molecules are bound to a small hydrophobic pocket, referred to as the αD pocket, located between the αD and 3_{10}-helices near the ribose-binding region [Fig. 1(*b*)]. This cluster of water molecules is likely to act as a damper for movement of the αD helix, which is a critical switch in CK2a1 to use either ATP or GTP as a phosphate source (Niefind *et al.*, 1999). Asp120 is likely to function as an N-cap residue (Richardson & Richardson, 1988) of the αD helix, which stabilizes the positive dipole moment of the α-helix structure.

3.2. Comparison of the binding modes of 5IOD between CK2a1 and other protein kinases

Besides the structure of CK2a1, five crystal structures of 5IOD–protein kinase complexes are available from the Protein Data Bank (Fig. 2). The interaction of 5IOD with the hinge region is essentially conserved in the structures of CK2a1, CK1g2, ERK1, ERK2, haspin and CLK1. The 4-aminopyrrolopyrimidine moiety of 5IOD binds at a similar position in all structures via three hydrogen bonds to the hinge region (Table 3). These interactions use main-chain atoms and are thus independent of differences in the amino-acid sequences (Fig. 2). The more bulky hydrophobic residues that form the C-spine narrow the ATP-binding site of CK2a1 when compared with those of other kinases (Fig. 2). Therefore,

Table 3
Inhibitory activities and/or binding dissociation constants of 5-iodotubercidin against the kinases and the number of electrostatic interactions.

Kinase	IC_{50} (μM)	K_d† (μM)	4-Aminopyrrolopyrimidine	Ribose	I atom
CK2a1	10.9†		3 hydrogen bonds	None	1 hydrogen bond
CK1g2	0.4†		3 hydrogen bonds	3 hydrogen bonds	1 hydrogen bond
ERK1	1.2‡		3 hydrogen bonds	3 hydrogen bonds	1 hydrogen bond
ERK2	0.9‡		3 hydrogen bonds	3 hydrogen bonds	1 hydrogen bond
Haspin	0.009§	0.006¶	3 hydrogen bonds	3 hydrogen bonds	1 hydrogen bond, 1 halogen–π interaction
CLK1		0.007¶	3 hydrogen bonds	3 hydrogen bonds	1 hydrogen bond, 1 halogen–π interaction

† Massillon *et al.* (1994). ‡ Kinoshita *et al.* (2008). § Balzano *et al.* (2011). ¶ Heroven *et al.* (2018).

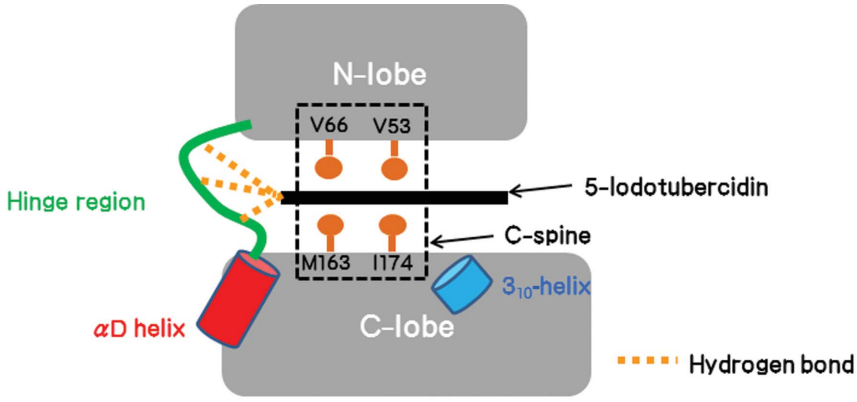

Kinase	PDB code	Upper of C-spine		Gatekeeper	Hinge region						N-cap of αD	Bottom of C-spine	
CK2a1	6JWA	V53	V66	F113	E114	H115	V116	N117	N118	T119	D120	M163	I174
CK1g2	2C47	L60	A73	L119	E120	L121	L122	G123	-	P124	S125	L172	I187
ERK1	2ZOQ	V56	A69	Q122	D123	L124	M125	E126	-	T127	D128	L173	C183
ERK2	5AX3	V30	A43	Q96	D97	L98	M99	E100	-	T101	D102	L147	C157
Haspin	3IQ7	V498	A509	F605	E606	F607	G608	G609	-	I610	D611	L656	I686
CLK1	6G33	V175	A189	F241	E242	L243	L244	G245	-	L246	S247	L295	V324

Figure 2
Amino-acid residues of the protein kinases involved in the interaction with the 4-aminopyrrolopyrimidine moiety of 5-iodotubercidin.

planarity of inhibitors is likely to be a structural requirement for CK2a1 selectivity.

The ribose moiety of 5IOD binds tightly to all kinases except CK2a1 (Table 3); the carbonyl group in the 3_{10}-helix and the side chains in the αD helix act as hydrogen-bond acceptors or donors. The αD helix of CK2a1 is displaced when compared with those of the other kinases and it cannot participate in hydrogen bonding to the ribose moiety (Fig. 3). In constrast, the configuration of the carbonyl group in the 3_{10}-helix is well conserved among these kinases (Fig. 3). However, Met163 of CK2a1 disturbs hydrogen bonding to the ribose moiety owing to steric hindrance (Fig. 3). Furthermore, Met163 is immobilized by the side-chain atoms of Asn118, which is a unique insertion residue in the hinge region. The structure revealed that Ile174, Met163 and Asn118 form a wider hydrophobic planar structure in the ribose-binding region of CK2a1 (Fig. 3).

The I atom of 5IOD faces the gatekeeper residue in all 5IOD complexes. The higher inhibitory activities of 5IOD for haspin and CLK1 are likely to be attributable to the halogen–π interaction between the gatekeeper phenylalanine residue and the I atom (Heroven *et al.*, 2018). Although the gatekeeper residue of CK2a1 is Phe113, as found in haspin and CLK1, this residue is distal from the I atom. The reduced interaction of the ribose and I atom of 5IOD with CK2a1 is most likely to account for the lower inhibitory activity of CK2a1 (Table 3). The values for the inhibitory activity and/or the binding dissociation constant extracted from previous reports (Massillon *et al.*, 1994; Kinoshita *et al.*, 2008; Balzano *et al.*, 2011; Heroven *et al.*, 2018) are associated with the number of electrostatic interactions involving hydrogen bonds and halogen–aromatic π interactions (Table 3).

The iodine-ligated W1 in the CK2a1 complex is conserved in the 5IOD complexes of CK1g2, ERK1, CLK1 and haspin. The low-resolution ERK2 structure contains no water molecules, but has sufficient space to be bound by a water molecule.

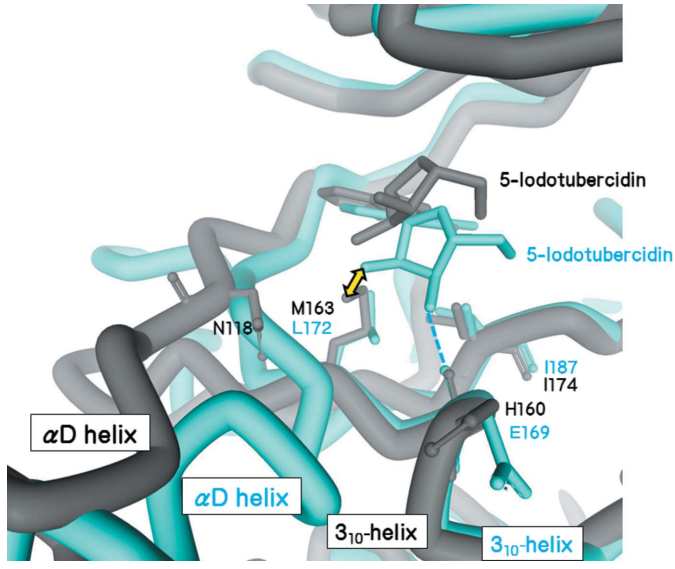

Figure 3
Superimposition of the 5-iodotubercidin complexes of CK2a1 (grey) and CK1g2 (blue). The ribose moiety in the CK2a1 complex is located in the upper position when compared with that of CK1g2. The position of the ribose moiety in the CK1g2 structure would cause steric clashes with Met163 of CK2a1 (yellow arrow).

The water molecule W0 is conserved in haspin but not in the other four kinases. Thus, the W0 position is unique and could be available for increasing the selectivity of CK2a1 inhibitors.

The αD pocket was observed in the CK2a1 complex but not in the other five kinases. The single insertion residue in the hinge region of CK2a1 probably impedes the formation of the zipper-like interaction between the αD and 3_{10}-helices that is observed in other kinase structures such as that of CK1g2 (Fig. 3). Thus, the αD helix of CK2a1 is located in the outer region and distal from the 3_{10}-helix. The space afforded by the position of the αD helix is occupied by Asn118 and water molecules (Fig. 3). αD pocket binders have recently been discovered (Iegre *et al.*, 2018) and are therefore suitable for producing highly selective CK2a1 inhibitors.

4. Conclusion

The 1.78 Å resolution structure of the 5IOD–CK2a1 complex and a comparative structural dissection of this structure and those of five other protein kinases provide structural insights for improving the inhibitory activity and selectivity of CK2a1 inhibitors. The hydrophobic regions of the ribose-binding site and the αD pocket are unique among protein kinases and are useful for structure-based drug discovery of CK2a1-selective inhibitors. Recently, Iegre and coworkers reported αD binders connected to an ATP-site inhibitor via a long flexible liker (Iegre *et al.*, 2018). Likewise, 5IOD could be merged with αD binders at the hydroxyl groups in the ribose moiety.

Acknowledgements

Preliminary experiments and diffraction data collection were carried out on beamline BL17A at the Photon Factory (Proposal No. 2016G665) and on the Osaka University beamline BL44XU at SPring-8 (Proposal No. 2017B6717). The authors thank Edanz Group (http://www.edanzediting.com/ac) for editing a draft of this manuscript.

References

Adams, P. D., Afonine, P. V., Bunkóczi, G., Chen, V. B., Davis, I. W., Echols, N., Headd, J. J., Hung, L.-W., Kapral, G. J., Grosse-Kunstleve, R. W., McCoy, A. J., Moriarty, N. W., Oeffner, R., Read, R. J., Richardson, D. C., Richardson, J. S., Terwilliger, T. C. & Zwart, P. H. (2010). *Acta Cryst.* D**66**, 213–221.

Balzano, D., Santaguida, S., Musacchio, A. & Villa, F. (2011). *Chem. Biol.* **18**, 966–975.

Duncan, J. S. & Litchfield, D. W. (2008). *Biochim. Biophys. Acta*, **1784**, 33–47.

Emsley, P., Lohkamp, B., Scott, W. G. & Cowtan, K. (2010). *Acta Cryst.* D**66**, 486–501.

Eswaran, J., Patnaik, D., Filippakopoulos, P., Wang, F., Stein, R. L., Murray, J. W., Higgins, J. M. G. & Knapp, S. (2009). *Proc. Natl Acad. Sci. USA*, **106**, 20198–20203.

Heroven, C., Georgi, V., Ganotra, G. K., Brennan, P., Wolfreys, F., Wade, R. C., Fernández-Montalván, A. E., Chaikuad, A. & Knapp, S. (2018). *Angew. Chem. Int. Ed.* **57**, 7220–7224.

Iegre, J., Brear, P., De Fusco, C., Yoshida, M., Mitchell, S. L., Rossmann, M., Carro, L., Sore, H. F., Hyvönen, M. & Spring, D. R. (2018). *Chem. Sci.* **9**, 3041–3049.

Kinoshita, T., Matsubara, M., Ishiguro, H., Okita, K. & Tada, T. (2006). *Biochem. Biophys. Res. Commun.* **346**, 840–844.

Kinoshita, T., Nakaniwa, T., Sekiguchi, Y., Sogabe, Y., Sakurai, A., Nakamura, S. & Nakanishi, I. (2013). *J. Synchrotron Rad.* **20**, 974–979.

Kinoshita, T., Sugiyama, H., Mori, Y., Takahashi, N. & Tomonaga, A. (2016). *Bioorg. Med. Chem. Lett.* **26**, 955–958.

Kinoshita, T., Yoshida, I., Nakae, S., Okita, K., Gouda, M., Matsubara, M., Yokota, K., Ishiguro, H. & Tada, T. (2008). *Biochem. Biophys. Res. Commun.* **377**, 1123–1127.

Massillon, D., Stalmans, W., van de Werve, G. & Bollen, M. (1994). *Biochem. J.* **299**, 123–128.

Miyano, N., Kinoshita, T., Nakai, R., Kirii, Y., Yokota, K. & Tada, T. (2009). *Bioorg. Med. Chem. Lett.* **19**, 6557–6560.

Murshudov, G. N., Skubák, P., Lebedev, A. A., Pannu, N. S., Steiner, R. A., Nicholls, R. A., Winn, M. D., Long, F. & Vagin, A. A. (2011). *Acta Cryst.* D**67**, 355–367.

Niefind, K., Pütter, M., Guerra, B., Issinger, O. G. & Schomburg, D. (1999). *Nature Struct. Biol.* **6**, 1100–1103.

Otwinowski, Z. & Minor, W. (1997). *Methods Enzymol.* **276**, 307–326.

Richardson, J. S. & Richardson, D. C. (1988). *Science*, **240**, 1648–1652.

Sekiguchi, Y., Nakaniwa, T., Kinoshita, T., Nakanishi, I., Kitaura, K., Hirasawa, A., Tsujimoto, G. & Tada, T. (2009). *Bioorg. Med. Chem. Lett.* **19**, 2920–2923.

Siddiqui-Jain, A., Drygin, D., Streiner, N., Chua, P., Pierre, F., O'Brien, S. E., Bliesath, J., Omori, M., Huser, N., Ho, C., Proffitt, C., Schwaebe, M. K., Ryckman, D. M., Rice, W. G. & Anderes, K. (2010). *Cancer Res.* **70**, 10288–10298.

Taylor, S. S. & Kornev, A. P. (2011). *Trends Biochem. Sci.* **36**, 65–77.

Vagin, A. & Teplyakov, A. (2010). *Acta Cryst.* D**66**, 22–25.

Yamada, M., Katsuma, S., Adachi, T., Hirasawa, A., Shiojima, S., Kadowaki, T., Okuno, Y., Koshimizu, T. A., Fujii, S., Sekiya, Y., Miyamoto, Y., Tamura, M., Yumura, W., Nihei, H., Kobayashi, M. & Tsujimoto, G. (2005). *Proc. Natl Acad. Sci. USA*, **102**, 7736–7741.